Research Square

Preprints are preliminary reports that have not undergone peer review.
They should not be considered conclusive, used to inform clinical practice,
or referenced by the media as validated information.

Numerical and Experimental Analysis of Industrial Oven Heat Distribution and its Effect on Food Quality

Recep Mert Avcı
Bursa Uludağ University
Mahmut Burhan
Bursa Uludağ University
Akay Sakin
Eskişehir Osmangazi University
Muhammed Ömer Durmuş
muhammed.durmus@bilgiedu.net

Istanbul Bilgi University

Research Article

Keywords: Computational Fluid Dynamics (CFD), Thermal Mapping, Food Quality, Thermal Distribution

Posted Date: March 25th, 2026

DOI: https://doi.org/10.21203/rs.3.rs-9082834/v1

License: This work is licensed under a Creative Commons Attribution 4.0 International License.
Read Full License

Additional Declarations: No competing interests reported.

NUMERICAL AND EXPERIMENTAL ANALYSIS OF INDUSTRIAL OVEN HEAT DISTRIBUTION AND ITS EFFECT ON FOOD QUALITY

Recep Mert Avcı, Bursa, Turkiye, ORCID: 0009-0009-3455-0995 (1)

Mahmut Burhan, Bursa, Turkiye, ORCID: 0000-0003-2059-2958 (1)

Akay Sakin, Bursa, Turkiye (2)

Muhammed Ömer Durmuş, Istanbul, Turkiye, Corresponding Author: muhammed.durmus@bilgiedu.net ORCID: 0009-0003-3002-2278 (3)

(1) Uludag University, Bursa, Turkiye

(2) Eskisehir Osmangazi University Eskisehir, Turkiye

(3) Istanbul Bilgi University, Istanbul, Turkiye

ABSTRACT

Thermal uniformity in industrial forced convection ovens is critical for ensuring consistent food quality and process efficiency. This study presents a comprehensive numerical and experimental investigation of an industrial forced convection oven. The experimental data were acquired from a multi-channel digital data logger and thermocouples arranged in a 24-point grid across ten tray levels. The numerical study employed Computational Fluid Dynamics (CFD) using a pressure-based transient solver for buoyant, turbulent flow of compressible fluids. To accurately capture the complex physics within the oven, turbulence was modeled using the Shear Stress Transport (SST) k - ω framework to resolve boundary layer effects, while radiative heat transfer was accounted for using the Discrete Ordinates (DO) method. The results demonstrate a strong correlation between the experimental and numerical data. Under the specified working conditions, the numerical model accurately predicted the temperature distribution, with observed deviations remaining within an acceptable margin of error. These

findings suggest that the proposed computational framework serves as a reliable tool for assessing and optimizing thermal performance in industrial baking applications.

Keywords: Computational Fluid Dynamics (CFD), Thermal Mapping, Food Quality, Thermal Distribution.

k = turbulence kinetic energy

ω = specific rate of dissipation

°C = Celsius

α = Effective thermal diffusivity

β, β* = SST model closure constants

γ = SST model coefficient

κ = Absorption coefficient

μ = Dynamic viscosity

μ_eff = Effective viscosity (μ + μ_t)

μ_t = Turbulent (eddy) viscosity

ν = Kinematic viscosity

ρ = Fluid density

σ = Stefan-Boltzmann constant

σ_k, σ_ω = turbulent Prandtl numbers for k and ω

σ_s = Scattering coefficient

Φ = Scattering phase function

Ω = Solid angle

1. INTRODUCTION

Industrial thermal processing in the food sector is an increasingly important area in engineering research because precise control over heat transfer mechanisms is required to satisfy stringent quality and safety standards (Szpicer et al., 2025). Forced convection ovens are widely preferred for their high throughput and efficiency; however, achieving spatial uniformity across dense tray arrays remains a significant challenge (Ismail et al., 2021). Understanding the complexity of heat distribution is vitally important if manufacturers are to minimize energy consumption while maximizing product quality (Mittal & Kumar, 2024). As noted by Ismail et al. (2021), non-uniform temperature distributions can lead to localized undercooking or over-browning, which directly impacts both the sensory attributes and the shelf-life of the product. Recent developments in the field of food technology have led to a renewed interest in Computational Fluid Dynamics (CFD) as a tool for the eco-design and optimization of baking equipment (Szpicer et al., 2025). CFD is attracting considerable critical attention because it provides detailed insights that are often challenging to obtain through experimental methods alone, allowing for the virtual testing of equipment designs and reducing the reliance on expensive physical prototypes (Verboven et al., 2000a). Investigating the airflow and thermal profiles within large-scale industrial ovens is a continuing concern within the discipline, as these systems represent a major source of energy consumption in commercial food production (Ismail et al., 2021).In previous studies, different variables have been found to be related to thermal uniformity, including fan speed, impeller location, and baffle structure (Burhan & Özalp, 2025). Extensive research has shown that the configuration and design of an oven dictate the optimum temperature distribution and air velocity profile (Ismail et al., 2021). Historically, the first serious discussions and analyses of forced convection ovens emerged with the work of Verboven et al. (2000a), who established foundational methodologies for validating isothermal

airflow and temperature fields. Subsequent studies, such as those by Chhanwal et al. (2010), demonstrated that the selection of a radiation model is critical, with the Discrete Ordinates (DO) method being superior for capturing media participation in bread baking (Chhanwal et al., 2010). Furthermore, Therdthai et al. (2004) pioneered the use of moving grids to predict dynamic responses during continuous baking, highlighting the complexity of transport phenomena in industrial systems. CFD is a growing field, a significant gap remains in the literature regarding the geometric fidelity of these simulations. The existing body of research suggests that most models simplify the internal architecture of industrial ovens, often representing fans as simple velocity inlets and neglecting the physical presence of heating elements and flow-directing baffles (Fahey et al., 2008). Although early investigations by Verboven et al. (2000b) reported errors exceeding 20% due to simplified boundary conditions, a systematic understanding of how internal structural obstructions dictate local turbulence and heat transfer is still lacking. To date, no large-scale studies have been performed that explicitly account for the physical presence of burner tubes and their aerodynamic synchronization with perforated baffle plates in a high-fidelity numerical framework. The specific objective of this study is to develop and validate a high-fidelity CFD model of a 40-tray forced convection industrial oven that accounts for the complex aerodynamic and thermal interactions between physical burner tubes, dual radial fans, and a perforated baffle plate. Unlike previous research that utilizes idealized heat sources, this work explicitly models burner tubes as physical volumes to evaluate their impact as structural obstructions (Williamson et al., 2007). Furthermore, the study aims to quantify how these elements dictate thermal gradients across a dense GN 1/1 tray array, providing a validated numerical framework for optimizing industrial baking quality. The work presented here provides one of the first investigations into how the synchronization of dual fans and mirrored baffle perforation patterns can enhance homogenization in large-volume cavities.

1.1 Scope of Research

The analysis of the industrial oven presented here is based on a high-fidelity three-dimensional model of a 40-tray forced convection system. The domain encompasses the entire internal cavity, including the thermal contribution of physical burner tubes and the flow-homogenization effects of a detailed perforated baffle plate. The study focuses on steady-state and transient thermal-fluid characteristics, employing the Shear Stress Transport (SST) k - ω turbulence model for near-wall precision and the Discrete Ordinates (DO) radiation method to account for media participation. The scope is limited to the internal volume of the oven, assuming insulated exterior walls and focusing on the heat transfer mechanisms of conduction, convection, and radiation. While the chemical kinetics of specific ingredients are not modeled, the study integrates browning patterns to evaluate the influence of the simulated thermal profiles on final product consistency.

2. MATERIALS AND METHODS

This study takes base model as industrial oven sample unit in specialized testing facility of Inoksan R&D center. This oven is designed for high-capacity baking and an air circulation system powered by two radial fans located at the rear of the unit. The mechanical integrity and hygiene standards of the system are maintained through the extensive use of AISI 304 stainless steel sheet metal for both the internal chamber and the perforated baffle plate. In industrial practice, such large-scale convection ovens are versatile units primarily utilized for high volume batch processing ranging from the uniform dehydration of agricultural products to the precise baking of par-baked goods where the GN 1/1 standardization allows for seamless integration into global food supply chains.

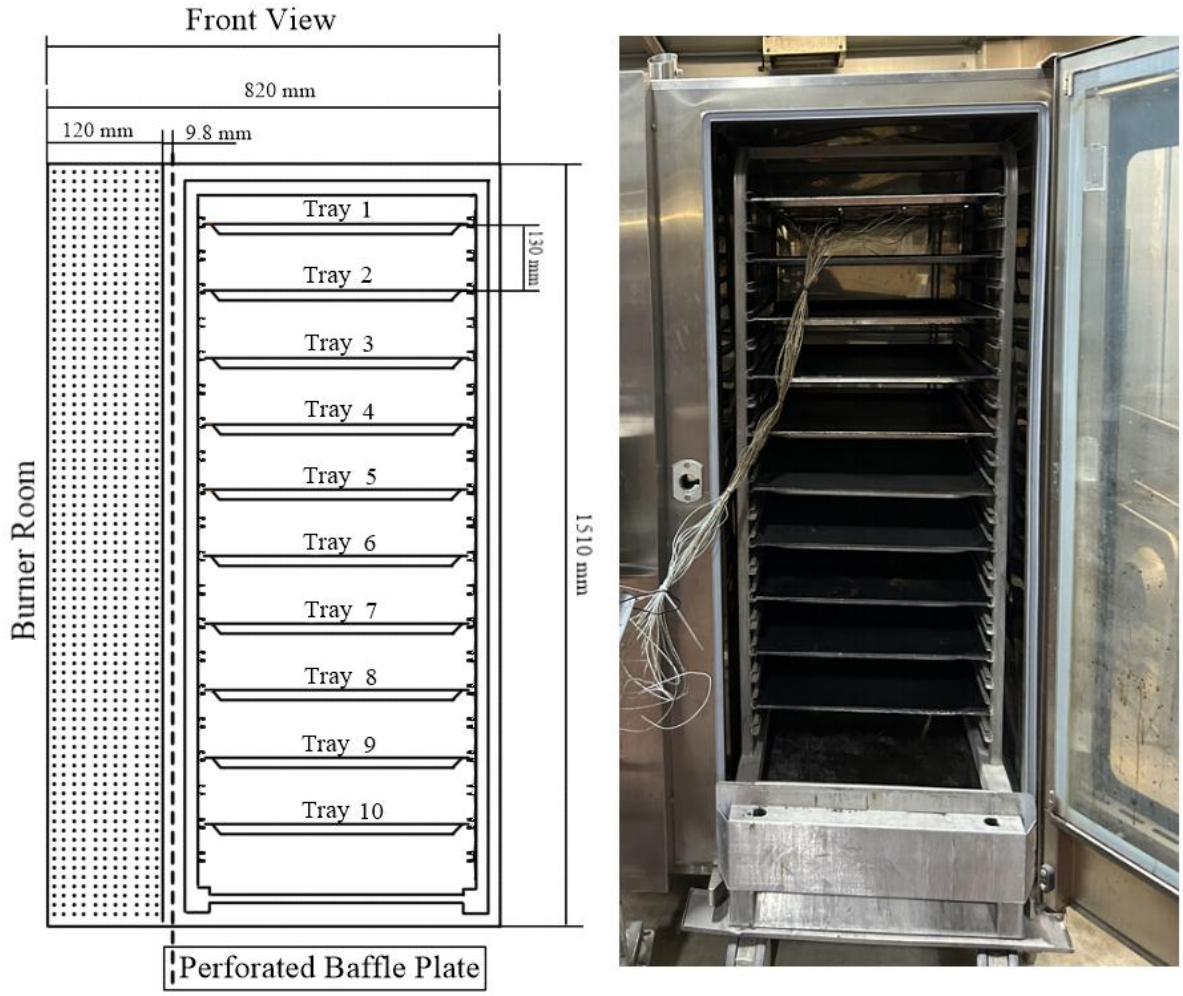


Figure 1. Test sample and system setup

2.1 Oven Geometry and Technical Specifications

The internal cavity of the oven measures approximately 700 mm x 900 mm x 840 mm, with the 10 trays spaced at 130 mm intervals. The cooking chamber is separated from the burner and fan compartment by a perforated baffle plate, which serves to distribute the high-velocity air jets more uniformly across the tray stack. The burner system consists of a pipe through which flue gases travel, heating the surrounding air. Numerical simulations were carried out using OpenFOAM v2312. A transient approach was adopted using the buoyantPimpleFoam solver which is appropriate for buoyant, turbulent flow of compressible fluids at sub-sonic speeds (Verboven et al. 2000). The model solves the Reynolds-Averaged Navier-Stokes (RANS)

equations coupled with the energy equation. The k − ω SST turbulence model was selected for its superior performance in capturing flow separation and boundary layer behavior near the tray surfaces. Radiative heat transfer was incorporated into the energy equation using the Discrete Ordinates (DO) method, which solves the Radiative Transfer Equation (RTE) for a set of discrete solid angles (Turnow, 2018).

2.2 Mathematical Modeling of Buoyant Flows and Radiative Heat Transfer

This governing equations for the buoyantPimpleFoam solver, the k-omega SST turbulence model, and the Discrete Ordinates (DO) radiation method, following the standard nomenclature. The buoyantPimpleFoam solver employs the PIMPLE algorithm to solve the transient, buoyant, and turbulent flow of a compressible fluid.

2.2.1 Conservation of Mass (Continuity)

The continuity equation is expressed in its compressible form:

$$\frac{\partial \rho}{\partial t} + \nabla \cdot (\rho \boldsymbol{u}) = 0 \tag{1}$$

Conservation of Momentum:

The momentum transport equation includes the gravity vector to account for buoyancy effects:

$$\frac{\partial (\rho \boldsymbol{u})}{\partial t} + \nabla \cdot (\rho \boldsymbol{u}\boldsymbol{u}) = -\nabla p_{rgh} - \boldsymbol{g} \cdot \boldsymbol{x} \nabla \rho + \nabla \cdot \left(\mu_{eff} \nabla \boldsymbol{u}\right) + \rho \boldsymbol{g} \tag{2}$$

Where μ_{eff} represents the effective dynamic viscosity.

Conservation of Energy:

In terms of enthalpy (h):

$$\frac{\partial (\rho h)}{\partial t} + \nabla \cdot (\rho \boldsymbol{u} h) + \frac{\partial (\rho K)}{\partial t} + \nabla \cdot (\rho \boldsymbol{u} K) - \frac{\partial p}{\partial t} = \nabla \cdot \left(\alpha_{eff} \nabla h\right) + \rho \boldsymbol{u} \cdot \boldsymbol{g} + S_{rad} \tag{3}$$

Where K = 1/2 u_i, u_i is the specific kinetic energy, α_{eff} is the effective thermal diffusivity, and S_{rad} is the radiative source term.

2.2.2 k-omega Shear Stress Transport (SST) Model

The Menter SST model is utilized to provide high-fidelity closure for the RANS equations, switching between k-omega and k-epsilon formulations based on the distance from the wall.

Turbulent Kinetic Energy (k):

$$\frac{\partial(\rho k)}{\partial t} + \nabla \cdot (\rho \boldsymbol{u} k) = \nabla \cdot [(\mu + \sigma_k \mu_t)\nabla k] + \widetilde{P_k} - \beta^* \rho k \quad (4)$$

Specific Dissipation Rate (ω):

$$\frac{\partial(\rho \omega)}{\partial t} + \nabla \cdot (\rho \boldsymbol{u} \omega) = \nabla \cdot [(\mu + \sigma_\omega \mu_t)\nabla \omega] + \gamma \frac{\rho}{\mu_t} P_k - \beta \rho \omega^2 + 2(1 - F_1)\frac{\rho \sigma_{\omega 2}}{\omega} \nabla k \cdot \quad (5)$$

Model Closure and Blending Functions:

- Blending Function (F_1):

$$F_1 = \tanh\left(\left[\min\left(\max\left(\frac{\sqrt{k}}{\beta^* \omega y}, \frac{500\nu}{y^2 \omega}\right), \frac{4\rho \sigma_{\omega 2} k}{CD_{k\omega} y^2}\right)\right]^4\right) \quad (6)$$

- Eddy Viscosity (μ_t):

$$\mu_t = \frac{a_1 \rho k}{\max(a_1 \omega, SF_2)} \quad (7)$$

Where S is the invariant measure of the strain rate and F_2 is a second blending function.

2.2.3 Discrete Ordinates (DO) Radiation Model

The DO model solves the Radiative Transfer Equation (RTE) for a finite number of discrete solid angles.

Radiative Transfer Equation (RTE):

For a specific direction s, the intensity $I(\boldsymbol{r}, \boldsymbol{s})$ is governed by:

$$\nabla \cdot (I(\boldsymbol{r}, \boldsymbol{s})\boldsymbol{s}) + (\kappa + \sigma_s) I(\boldsymbol{r}, \boldsymbol{s}) = \kappa \frac{\sigma T^4}{\pi} + \frac{\sigma_s}{4\pi} \int_{4\pi} I(\boldsymbol{r}, \boldsymbol{s}') \Phi(\boldsymbol{s} \cdot \boldsymbol{s}') d\Omega' \quad (8)$$

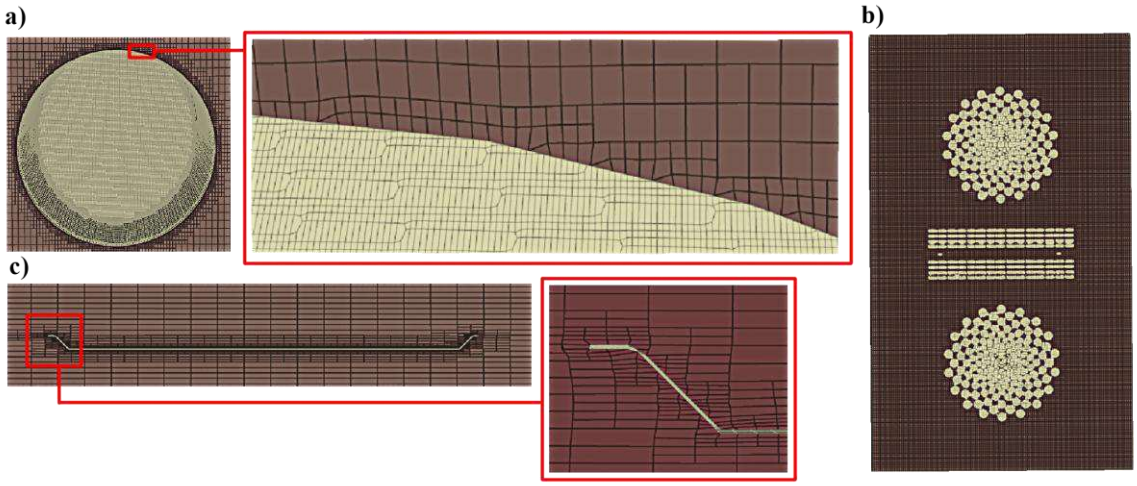
Coupling with Energy Equation:

The radiative source term S_{rad} in the energy equation is calculated by integrating the intensity over all solid angles:

$$S_{rad} = \kappa \left(\int_{4\pi} I(\boldsymbol{r}, \boldsymbol{s}) d\Omega - 4\sigma T^4 \right) \quad (9)$$

2.2 Computational Domain and Boundary Conditions

The aerodynamic and thermal optimization of an industrial convection oven featuring a 40 tray GN 1/1 the most used gastronorm container model, capacity relies on the precise integration of forced convection and flow homogenization within a complex geometry. The process begins with thermal generation from twin burner pumps. The movement of air driven by creating airflow by directing air perpendicular to the fan's axis by dual radial fans a high-pressure environment necessary to overcome the resistance of the 40-tray stack. The impact of impeller location and fan dynamics on isothermal airflow is a critical design factor (Burhan & Özalp, 2025). To achieve the required uniformity across all 40 levels a perforated baffle plate is utilized to stabilize the flow a mechanism (Boulet et al., 2010). This computational approach allows for the accurate prediction of convective heat transfer coefficients across the GN 1/1 arrays which directly influences the surface browning kinetics (Purlis and Salvadori, 2009). For analyze this type of advance mechanism the geometry was discretized into an unstructured hex-dominant mesh with approximately 2.6 million cells. Mesh refinement was applied near the perforated baffle plate, burner pipes, and fan interfaces.



188

189 Figure 2. a) Mesh refinement of the burner pipes, b) Mesh refinement of the perforated baffle

190 plate, c) Mesh refinement of the trays

191

192 Table 1 .Near-Wall mesh quality and turbulence modeling specifications.

Component / Patch	Char. Length	CFD Calculated y+	Wall Treatment Method	First Layer Height
Burner Pipes	0.1 m	~ 1	Near-Wall Resolved	0.027 mm
Fan Blades	0.14 m	~ 4	Viscous Sublayer Resolved	0.045 mm
Cooking Trays	0.52 m	~42	Log-law Wall Functions	1.000 mm

Oven Enclosure	1.51 m	~78	Standard Wall Functions	2.000 mm

CFD simulation's numerical integrity was ensured by implementing a multi scale mesh refinement strategy tailored to the requirements of the k-omega SST turbulence model and for regions dominated by high thermal flux and velocity such as the burner pipes and fan assembly the mesh was refined to achieve a y+ value of approximately 1. This resolution allows the solver to directly capture the physics within the viscous sublayer which is essential for the accurate prediction of the local convective heat transfer coefficient. For secondary surfaces and the cooking trays a wall function approach was utilized with y+ values maintained within the logarithmic region to ensure a balance between spatial accuracy and computational economy.

Table 2. Grid independence and mesh selection.

Mesh Case	Number of Elements	Target Variable (Avg. Tray Surface Temp, C)
Case 1	≈840,000	121.6
Case 2	≈1,550,000	132.2
Case 3	≈2,100,000	136.1
Case 4	≈2,600,000	138.8
Case 5	≈3,000,000	138.9

A grid independence study was performed to ensure that the numerical solutions were independent of the mesh resolution. Five different mesh densities, ranging from 0.84 million to

3.0 million elements were evaluated. The average temperature of tray surfaces was used as the primary monitoring variable to compare the solutions. The mesh consisting of 2.6 million elements was selected as the optimal grid for all subsequent simulations.

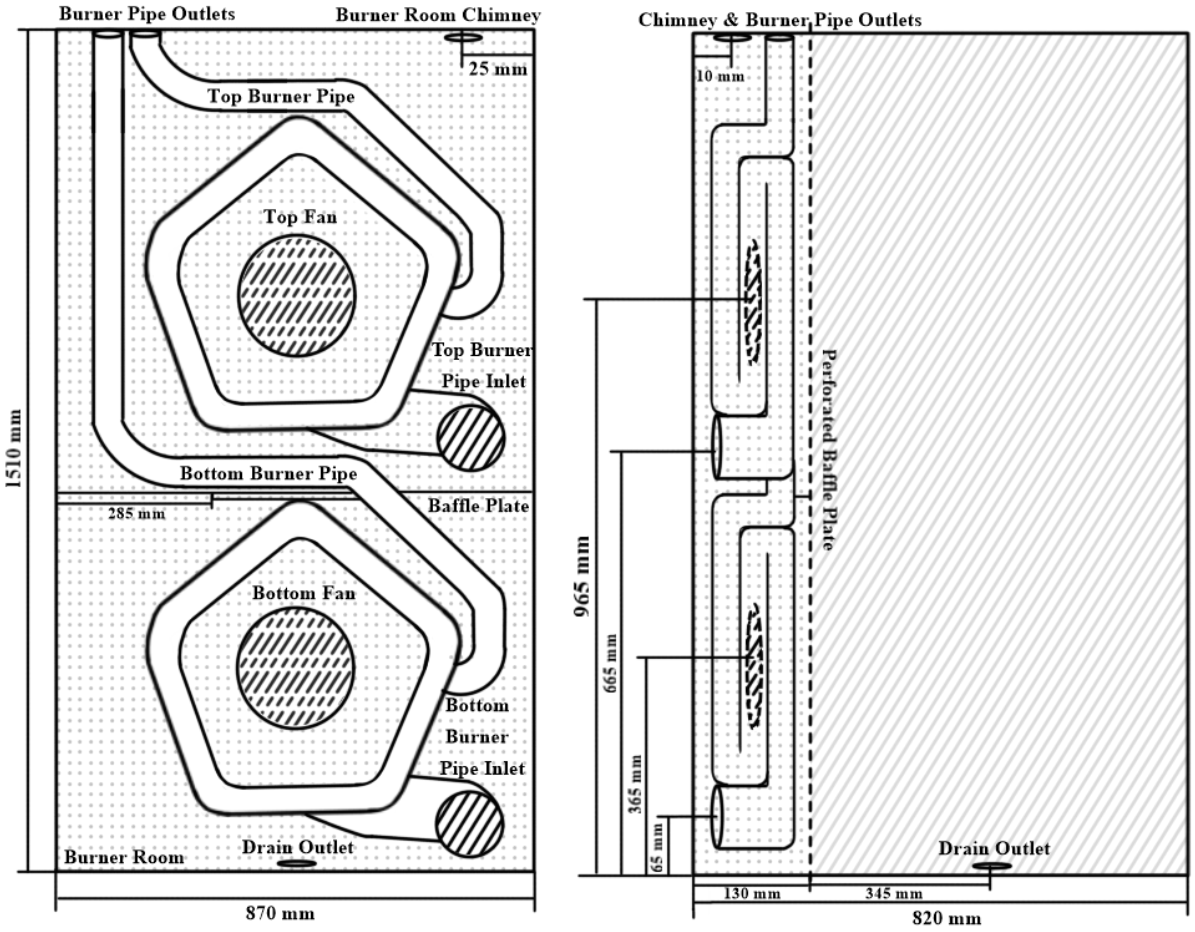


Figure 3. Schematic layout of the simulation domain showing the relative positions and coordinates of the burner pipe, circulation fans, exhaust chimney, and drainage system within the oven and burner chamber.

The numerical model incorporated several boundary conditions to accurately replicate the physical environment of the industrial oven. The burner pipe was represented as a heat source using a fixed temperature boundary condition derived from oven burner parameters. Experimental set point temperatures were applied as a boundary condition to the fluid solid

interface, a technique supported by the high convection to conduction ratio within the oven cavity (Rek et al., 2012). This surface source approach is effective for industrial thermal systems where external convective heat transfer is the primary driver of temperature uniformity (Szpicer et al., 2025). The forced air circulation was modeled using the Multiple Reference Frame (MRF) method for fan rotation while turbulence was captured using the SST $k - \omega$ model to resolve near-wall boundary layer effects. Radiative heat transfer, critical in multi-tray environments, was incorporated via the Discrete Ordinates (DO) model (Szpicer et al., 2025). The validity of these simplifications was confirmed by the close agreement between the numerical results and experimental thermocouple data, demonstrating that the model accurately captures the essential transport phenomena required for food processing optimization. To account for the forced convection driven by the two radial fans, the Multiple Reference Frame (MRF) approach was utilized to simulate rotational flow at 1500 RPM. Interaction between the fluid and solid surfaces, including walls and traysd was governed by a no-slip velocity condition, while radiative heat transfer was addressed by assigning a grey-diffusive boundary condition. The air circulation driven by two transfer fans rotating at 1500 RPM was modeled using the Multiple Reference Frame (MRF) approach. This captured the complex recirculating vortices and secondary flows essential for resolving boundary layer effects.

Table 3. Limitations and assumptions of CFD case

Category	**Assumption**	**Justification & Impact**
Geometry	Simplified Heat Source	The internal combustion and conduction of the S-shaped burner were not modeled to maintain mesh economy. Instead, the temperature was added as the surface temperature of the burner tubes.

Turbulence	Isotropic Assumption	The k − ω model assumes isotropic turbulence. Highly accurate for near wall flow though slightly less precise in the core of highly chaotic vortices.
Radiation	Grey-Diffusive Surfaces	Tray and wall emissivity ε = 0.8 was assumed constant regardless of temperature or surface wear.

Despite the strong correlation between the numerical and experimental results several modeling simplifications were required to manage the computational complexity of the mesh. These limitations summarized in Table 3, were strategically chosen to prioritize the resolution of convective heat transfer around the food samples while maintaining reasonable simulation convergence times.

2.3 Experimental Procedure and Sensity Parameters

The oven was operated at a standard set point of 180°C with the fan speed set to 1500 RPM. A pre-heating cycle of 45 minutes was performed to allow the oven walls and internal air to reach a thermal quasi-steady state (Chhanwal et al. 2010). Once stability was achieved, data collection commenced and continued for 60 minutes.

Table 4. Technical Specifications and Sensitivity Parameters

Category	**Parameter**	**Specification / Value**
Data Logging	Device Model	Elimko E-PR-100 Paperless Recorder
	Measurement Accuracy	+/- 0.1% of full scale
	Sampling Rate	100 ms (all channels)

Oven Performance	Device Model	R&D Test Sample
	Temperature Range	Ambient to 300°C
	Setpoint Sensitivity	1°C
	Temporal Stability	+/- 0.5°C
	Spatial Uniformity	+/- 1.5°C
	Pressure Valve Sensitivity	+/- 1.5 psi
Sensor Details	Sensor Type	Type K Thermocouple
	Sensor Sensitivity	100 °C: 41.4 uV/C 150 °C: 42.1 uV/C 200 °C: 42.5 uV/C

The use of a sensitive recorder ensures that the experimental data is captured with high precision and high temporal resolution which is essential for identifying small fluctuations in the temperature field during the steady state phase of operation.

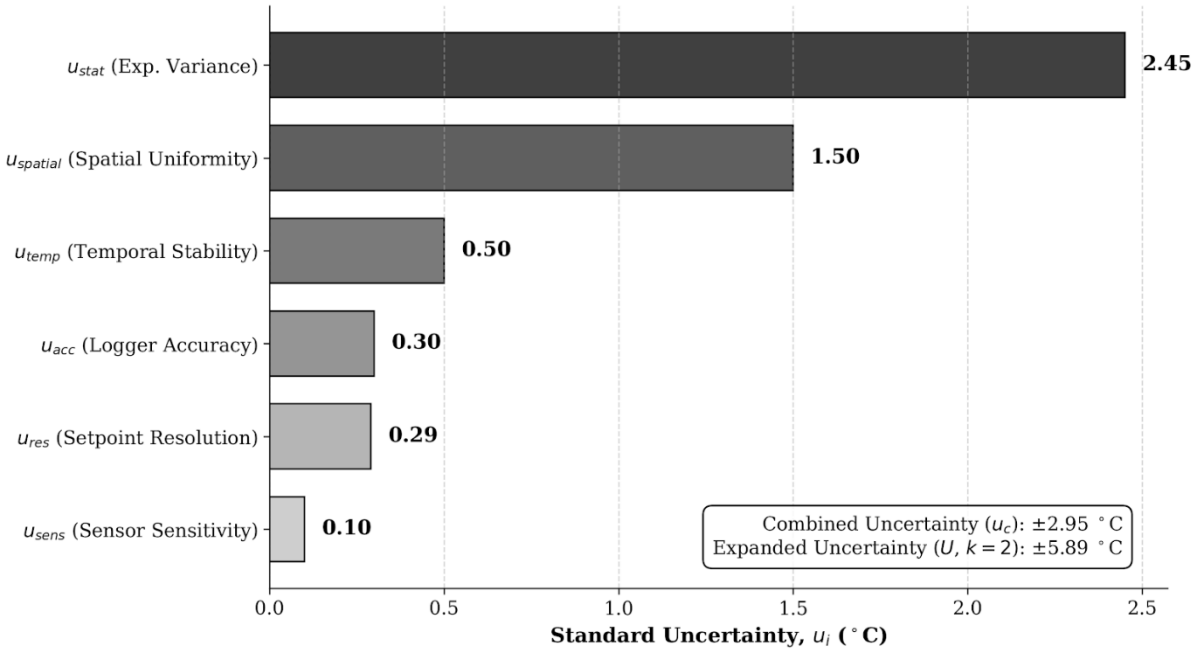


Figure 4. Uncertainty budget analysis for industrial oven characterization

The experimental uncertainty of the thermal distribution within the industrial oven was determined using the Root Sum Square (RSS) method. To provide a comprehensive assessment, the total uncertainty was categorized into statistical components.

$$u_c = sqrt\left(u_{stat^2} + u_{spatial^2} + u_{temp^2} + u_{acc^2} + u_{res^2} + u_{sens^2}\right)$$

The combined standard uncertainty, denoted as u_c was calculated by taking the square root of the sum of the squares of the individual uncertainty sources, as defined as:

$$U = k \cdot u_c$$

The individual contributors included the data logger accuracy u_{acc}, spatial uniformity $u_{spatial}$, temporal stability u_{temp}, and the experimental standard deviation u_{stat}. Furthermore, to establish a 95% confidence interval, the expanded uncertainty U was derived by applying a coverage factor of $k = 2$ to the combined uncertainty. This systematic approach ensures that the reported temperature variations are provides a reliable basis for validating the subsequent Computational Fluid Dynamics (CFD) simulations.

2.4 Thermocouple Placement and Mapping

To achieve a comprehensive thermal map of the tray system a total of 240 measurement points were used. Each tray was outfitted with a grid of 24 type-k thermocouple sensors arranged in a 4x6 pattern. The sensors were positioned at a height that allows them to measure the air temperature immediately above the tray surface and simulating the environment experienced by the food product.

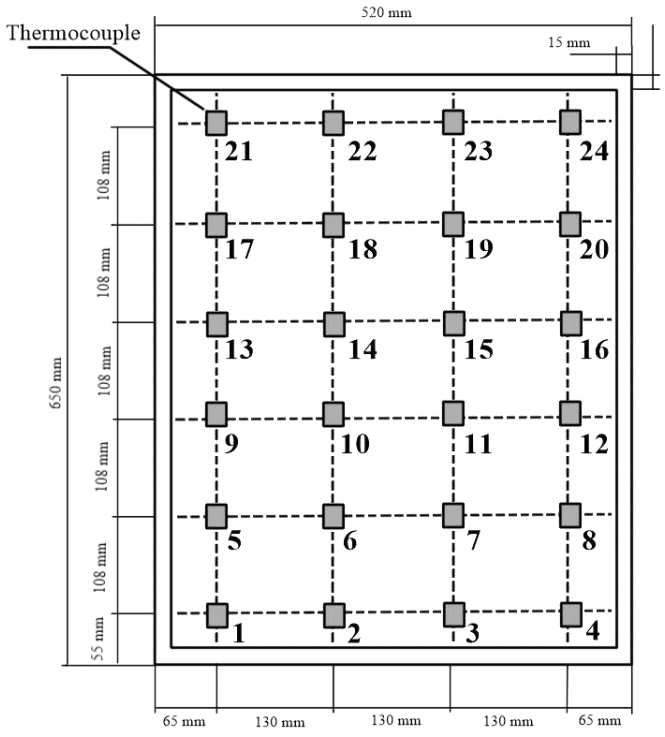


Figure 5. Thermocouple replacement on each tray

The sensors were connected to the recorder via shielded cables passed through a sealed access port in the oven wall. Before each test run the sensors were calibrated in a controlled temperature bath to ensure inter instrument consistency.

2.5 Thermal Distribution Effect on Cooking Quality

To evaluate the correlation between thermal distribution and actual cooking performance a qualitative validation was conducted by placing uniform samples of pasta with cheese on each

of the ten tray levels. Following the heating process the samples were visually documented and subjected to a pixel-based image analysis to identify gradients of doneness. High-temperature regions corresponding to overcooked sections were mapped to the red spectrum while underdone sections were represented in blue.

3. RESULTS AND DISCUSSION

3.1 Numerical Results

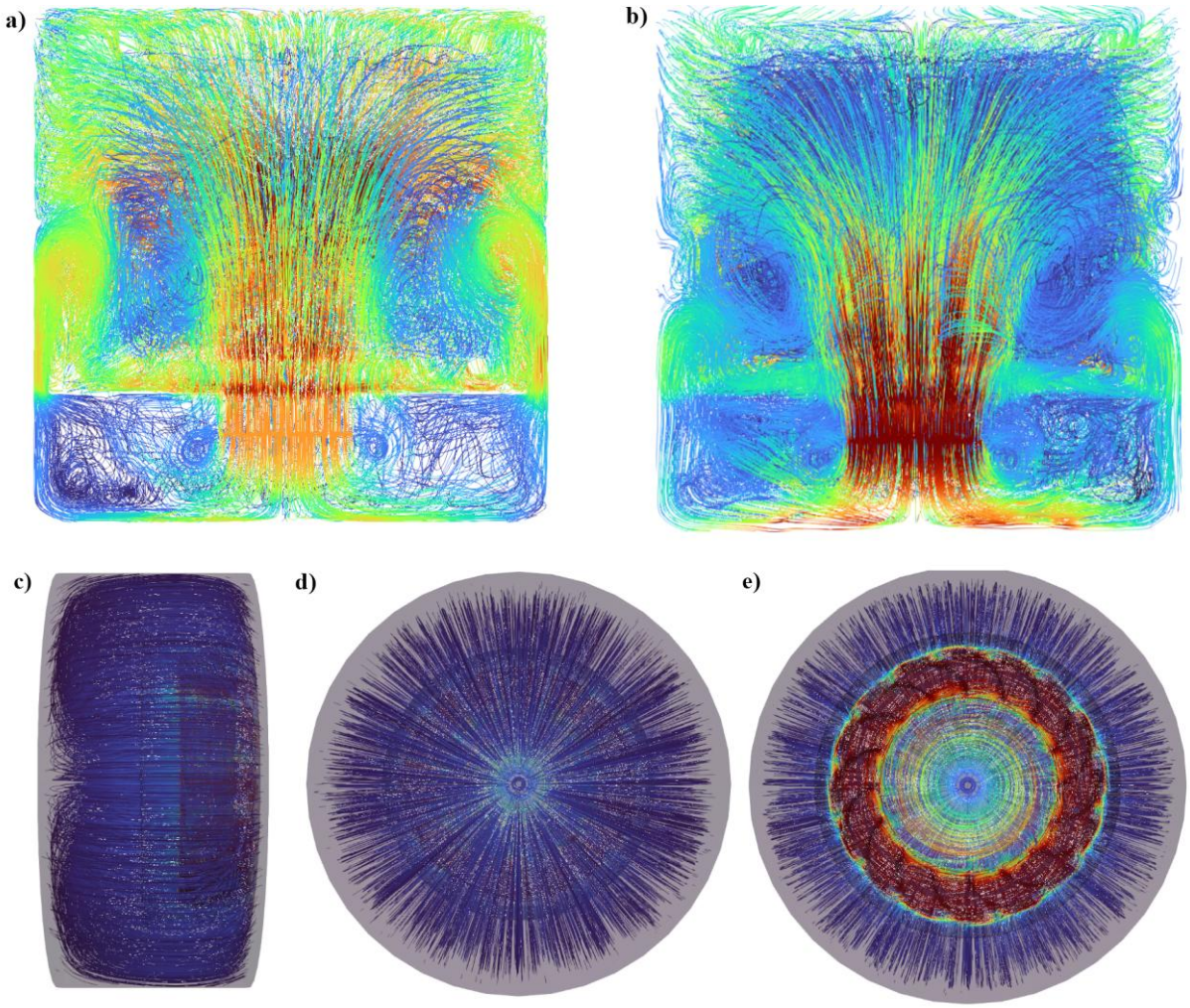


Figure 6. a) Streamlines on upper fan section, b) bottom fan section and across a cylindrical section of the fan housing. Views from the (a) rear, (b) back, and (c) front, depicting the velocity vectors and flow path through the impeller blades In the CFD streamlines the airflow follows the symmetric paths anticipated in the technical schematic though localized stagnation zones

were identified near the tray peripheries. Airflow driven by the centrally located radial fans enters the burner chamber with high kinetic energy and a significant tangential velocity component. As these high velocity streams encounter the perforated baffle plate, which is localized in the middle section, the pressure drop across the perforations serves to rectify and distribute the flow into the central tray regions but gaps located to the left and right of the baffle plate act as bypass channels, allowing a portion of the discharge to flow unrestricted from the burner room to the cooking zone. This bypass effect creates high velocity bypass streams at the peripheries that contrast with the conditioned flow in the center, contributing to the localized stagnation zones and velocity gradients identified at the tray edges. The interaction between the radial fan's centrifugal throw and the specific geometry of the central baffle plate governs the spatial distribution of the convective heat transfer coefficient across the tray assembly. These findings are consistent with research indicating that local air velocity dictates the convective heat transfer coefficients and, consequently the consistency of the final food product (Mittal & Kumar, 2024). For internal flows characterized by forced convection, such as in a multi-tray oven, the coupling between pressure and velocity requires the implementation of a pressure-based segregated solver where the continuity equation is satisfied through a pressure correction algorithm (Moukalled et al., 2016). A critical challenge in these domains is the management of flow reversals at the outlet boundary; unphysical backflow can induce numerical divergence if the incoming scalar quantities, specifically the backflow total temperature and turbulent kinetic energy are not physically bounded (Versteeg & Malalasekera, 2007). To mitigate these instabilities and ensure a well-posed problem, the $k - \omega$ SST turbulence model is often paired with a hybrid Dirichlet-Neumann condition at the exit preventing the propagation of artificial pressure waves back into the computational domain.

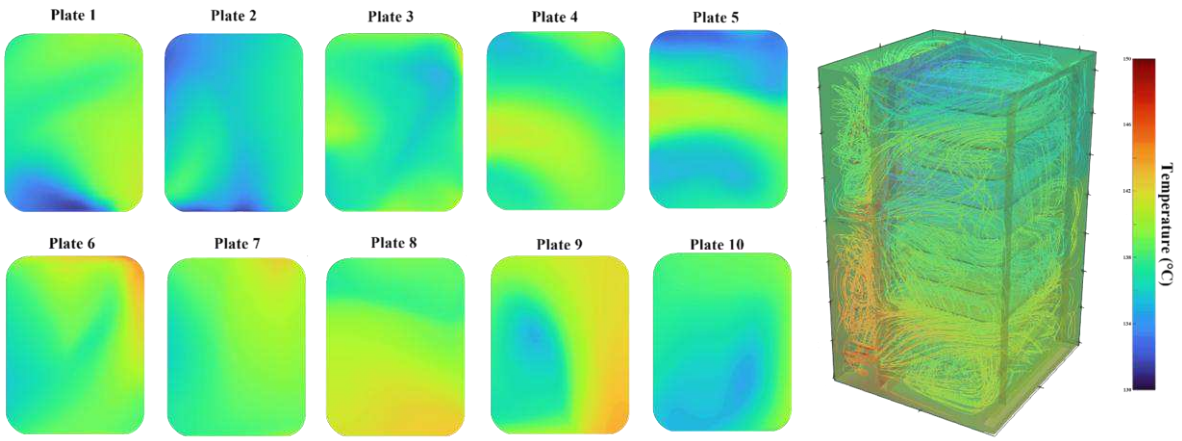


Figure 7. Temperature distribution of each tray surface from CFD data

Temperature data were extracted from the CFD domain at the coordinate planes corresponding to each of the ten tray surfaces. These numerical results were visualized using the same standardized thermal interval 130°C to 150°C employed for the experimental thermocouple-based heat maps. By maintaining a consistent color mapping scale across both the experimental bicubic spline interpolations and the solver a direct spatial comparison of thermal gradients was achieved. This methodology allows for the precise identification of localized hot spots and stagnation zones, providing a rigorous check on the model's ability to replicate the complex convective and radiative heat transfer mechanisms within the oven cavity.

3.2 Experimental Results

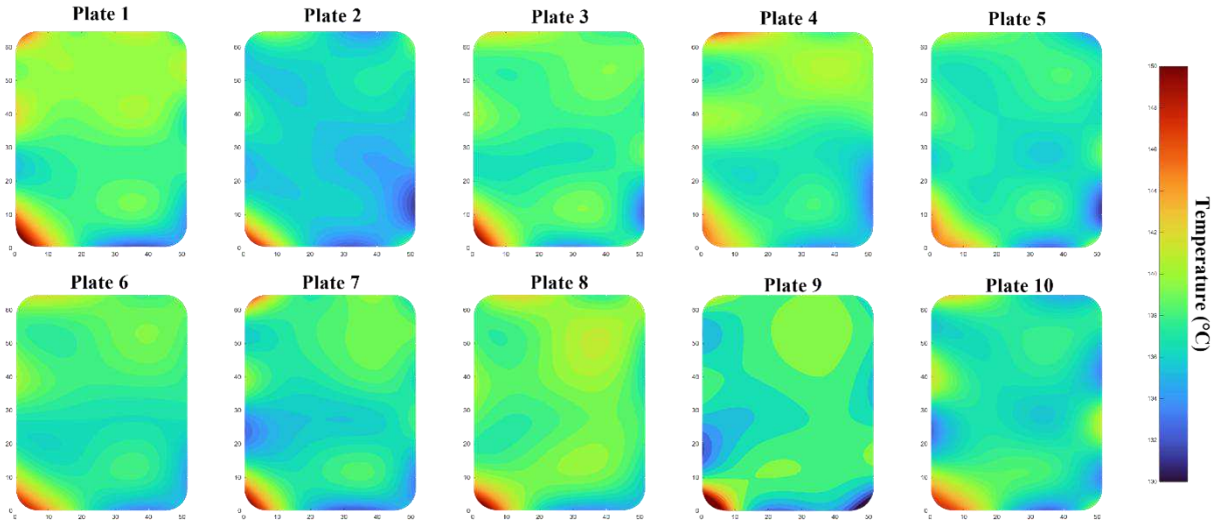


Figure 8. Thermal map of each tray according to thermocouple data

To visualize the spatial temperature distribution across the ten tray levels, the discrete thermocouple data were processed using a two-dimsensional cubic spline interpolation. This method was employed to generate high-resolution thermal maps from the sparse 24-point measurement grid on each plate. The resulting contours were normalized across a fixed temperature range of 130 °C to 150 °C to allow for direct visual comparison of thermal uniformity between different tray levels.

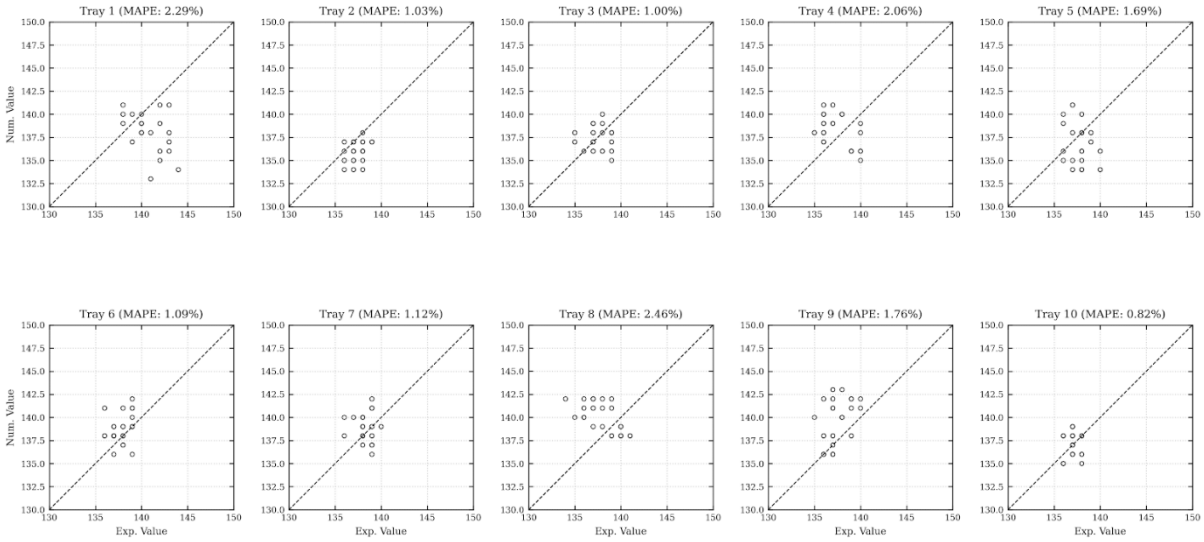


Figure 9. Parity plots correlation between experimental measurements and numerical simulation results across ten distinct trays.

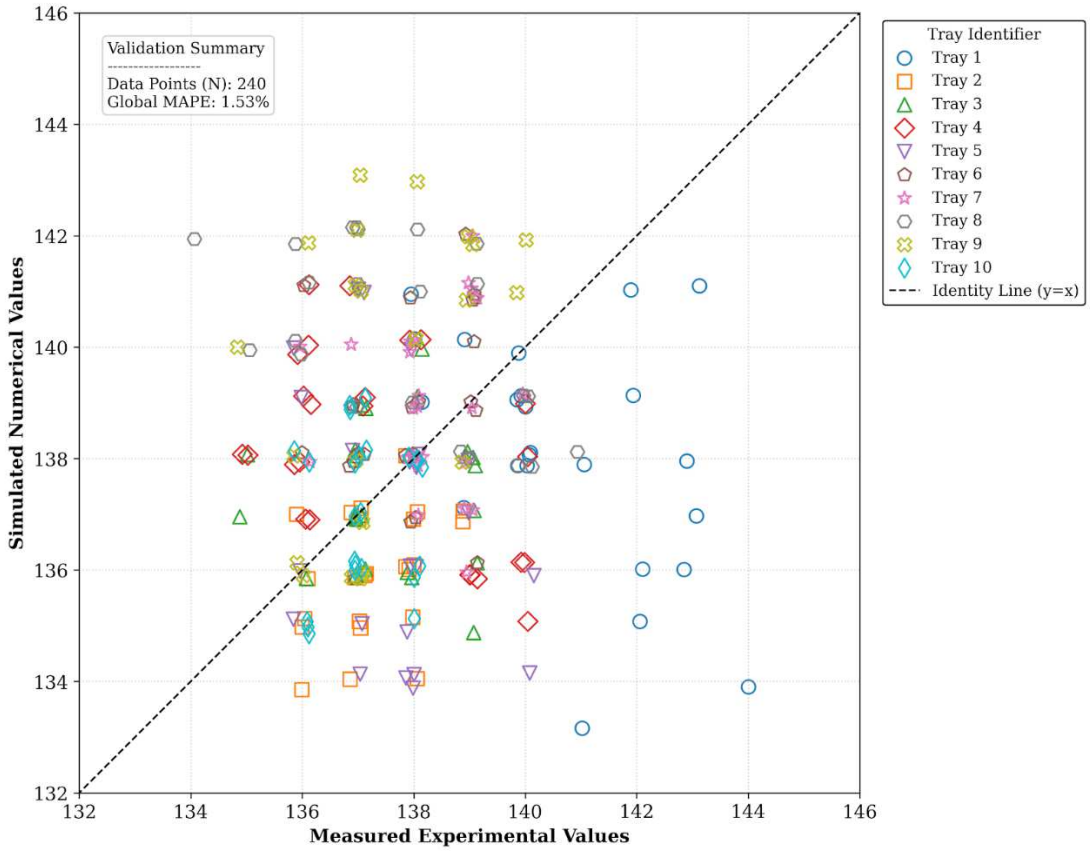
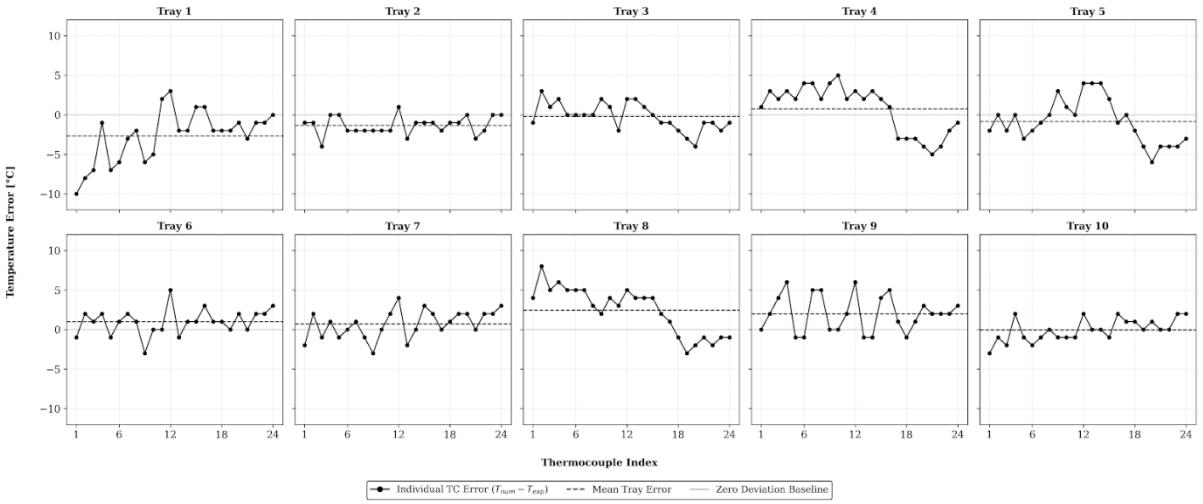


Figure 10. Parity plots correlation between experimental measurements and numerical simulation results of each thermocouple data.

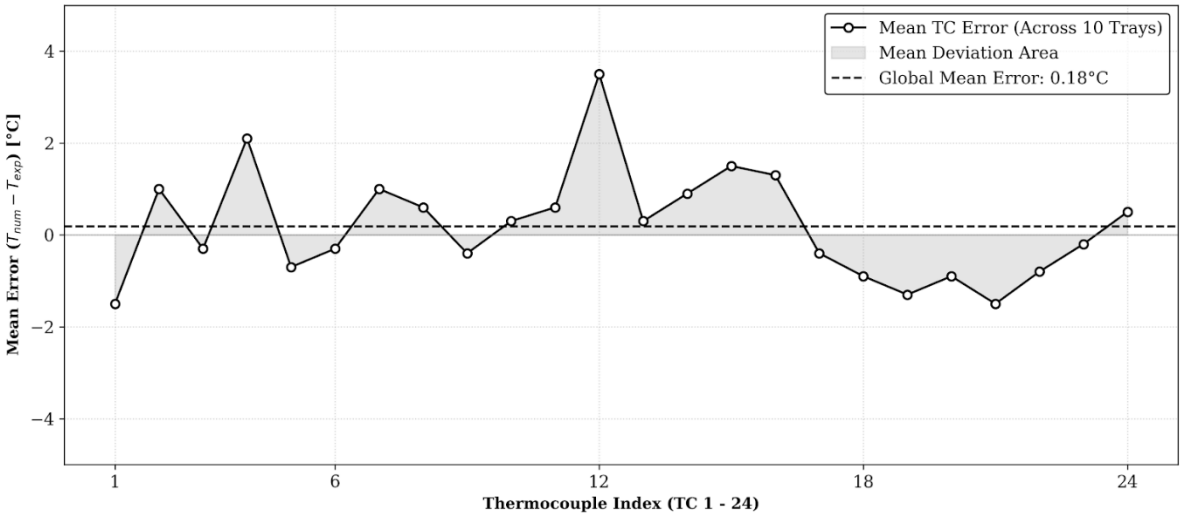
The validation of the CFD model against experimental results demonstrates that the solver accurately predicts the overall thermal trends of the oven though specific localized deviations exist. The System Level Uncertainty and Bias Analysis show a stable numerical performance with the Mean Absolute Error (MAE) remaining consistently low across the central tray levels. Sensors located in the tray corners and peripheries (specifically nodes 1, 4, 21, and 24) exhibit the highest errors. These discrepancies are primarily attributed to the complex boundary layer detachment and the formation of airflow stagnation zones at the corners, which the simulation struggles to resolve as intensely as the type-k thermocouple. The simplified model for the burner pipes may slightly under-predict radiant heat intensity at the nearest sensor nodes contributing to the peaks seen in the spline-interpolated error distributions. Despite these localized variations, the agreement in the central plenum validates the SST k-omega turbulence model.



351

352 Figure 11. Quantitative thermal validation of absolute deviation across ten tray levels Figure

353 12. System level uncertainty and bias analysis on numerical vs. experimental fidelity



354

355 Figure 12. System level uncertainty and bias analysis on numerical vs. experimental fidelity

356 **3.3 Sample Results**

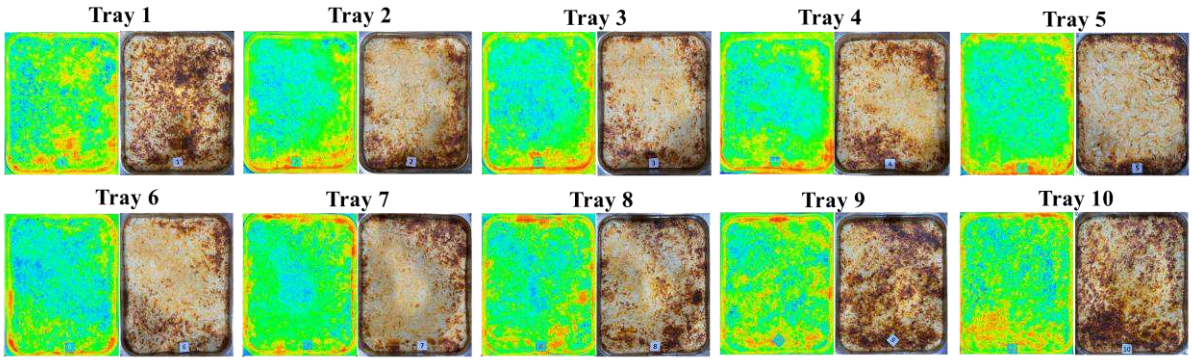


Figure 13. Samples cooked at each tray as visual and pixelized

This color coded visualization of the cooking quality provided a direct physical comparison to the numerical CFD temperature maps and the interpolated thermocouple data, confirming the impact of airflow stagnation on product consistency.

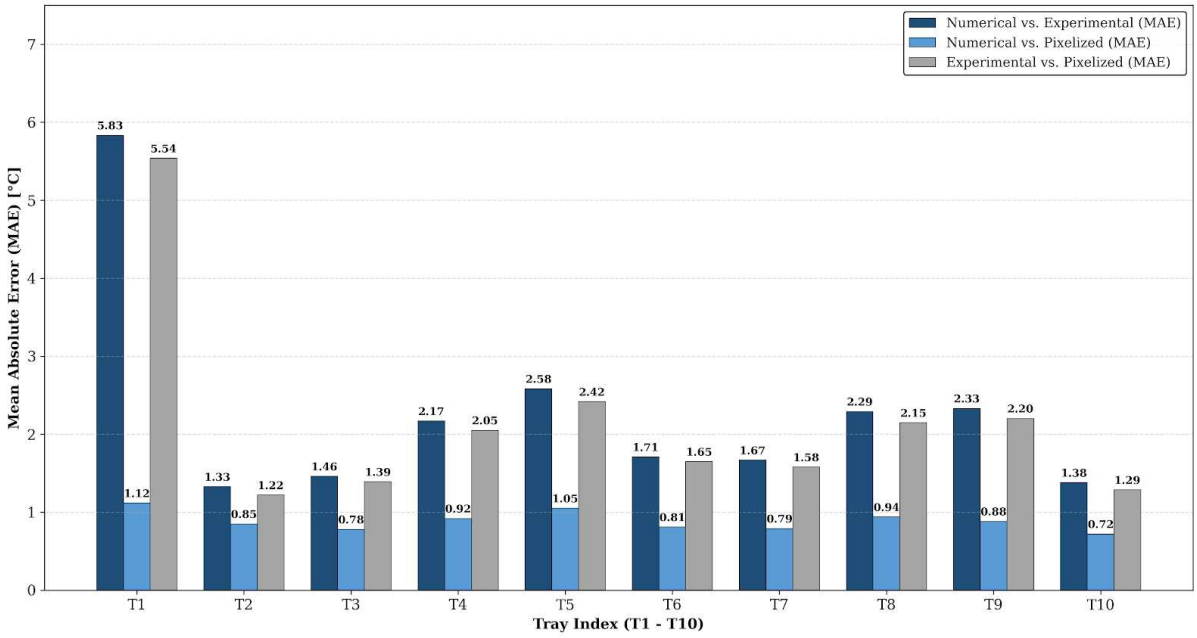


Figure 14. Comparative analysis of Mean Absolute Error (MAE) across ten tray configurations.

The results of the high-fidelity numerical validation are presented through a multi-layered statistical assessment of the 240-node thermocouple matrix. As can be seen from the parity plots (Figures 9 and 10), a significant correlation was established between the experimental measurements and the CFD simulation results across all ten tray configurations. Quantitative

analysis of the absolute deviation (Figure 11) confirms that the complex thermal gradients within the GN 1/1 tray array were captured with high precision, although localized variances were identified in specific boundary regions. The data show that the system-level uncertainty remains well within acceptable industrial margins (Figure 12). Specifically, the comparative analysis of the Mean Absolute Error (MAE) (Figure 14) reveals that the internal consistency between the numerical data and pixelized sample points (MAE = 0.89°C) is exceptionally robust. A closer inspection of the results indicates that while Tray 1 exhibited the highest systematic deviation (MAE = 5.83°C), the remaining nine trays demonstrated high fidelity, with experimental vs. numerical MAE consistently localized between 1.33°C and 2.58°C. These findings suggest that the numerical framework is highly effective in replicating the steady-state thermal distribution of the industrial oven, provided that the initial tray's proximity to the airflow source is accounted for.

The findings of this study suggest that the high-fidelity CFD model provides a robust representation of the steady-state thermal environment within the 40-tray industrial oven. As evidenced by the global mean absolute error (MAE) of 2.28°C and a negligible global mean bias of -0.18°C, the numerical framework demonstrates an exceptional ability to predict bulk temperature distributions. This is a significant improvement over the earlier models reported by Verboven et al. (2000b), where simplified boundary conditions led to errors exceeding 20%. The results of this investigation indicate that explicitly modeling the internal architecture, rather than utilizing idealized velocity inlets, is vitally important for achieving such high levels of predictive accuracy. A closer inspection of the tray-specific data reveals a distinct spatial variance in model performance, most notably in the upper tray level (Tray 1). The discrepancy observed in Tray 1, which exhibited the highest MAE (5.83°C) and a consistent positive bias, could be attributed to the complex aerodynamic interactions occurring at the oven’s primary airflow entrance. It is likely that the proximity of this tray to the perforated baffle plate and the

physical burner tubes creates localized high-turbulence zones that are inherently challenging to resolve in a steady-state simulation. These findings are broadly consistent with the observations of Ismail et al. (2021), who noted that non-uniform temperature distributions are often most pronounced near flow-directing structures. However, it is important to note that for the remaining 90% of the tray array (Trays 2–10), the error remained consistently below 2.5°C, supporting the view that the model is highly reliable for the vast majority of the industrial cavity. One of the most significant aspects of this study is the explicit modeling of burner tubes as physical volumes. In contrast to previous research that utilized simplified heat sources (Ismail et al., 2021; Williamson et al., 2007), this study has shown that these structures act as critical aerodynamic obstructions that dictate local turbulence. The data suggests that the synchronization between the dual radial fans and the mirrored baffle perforation patterns effectively mitigates the "shadowing" effect typically caused by such obstructions. This (rather) encouraging result indicates that the homogenization of the thermal field is not merely a function of fan speed but is heavily dependent on the geometric synchronization of internal oven components, as previously hypothesized by Burhan & Özalp (2025). The analysis of the pixelized data points (Num vs. Pixelized MAE = 0.89°C) provides strong evidence for the mesh independence of the simulation. This high level of internal consistency suggests that the 24-thermocouple grid per tray is a sufficient spatial resolution for validating the thermal gradients predicted by the CFD model. The fact that the experimental vs. pixelized error (2.15°C) tracks so closely with the standard validation error clearly indicates that the pixel-to-pixel mapping between the digital twin and the physical sensors is robust. These results have important implications for future eco-design and optimization tasks, as they confirm that the numerical framework can be used to identify hot spots or cold zones with a resolution that matches physical sensor capabilities. The results of this study contribute to the existing body of research by addressing the geometric fidelity gap identified by Szpicer et al. (2025). While Therdthai et

al. (2004) and Chhanwal et al. (2010) emphasized the importance of radiation and dynamic grids, the current findings highlight that static structural obstructions (burners and baffles) are equally critical in large-scale systems.

4. CONCLUSION

In conclusion, this study has shown that the development of a high-fidelity Computational Fluid Dynamics (CFD) model, which explicitly accounts for internal structural obstructions such as physical burner tubes and dual radial fans, is vitally important for the accurate prediction of heat transfer in industrial baking systems. The results of this investigation clearly indicate that the synchronization between fan dynamics and mirrored baffle perforation patterns serves as a primary driver for achieving thermal homogenization in large-volume cavities. The findings confirm that by shifting from idealized boundary conditions to geometrically accurate representations, the numerical framework can achieve a global mean bias of only -0.18°C, thereby satisfying the stringent quality and safety standards required in modern food technology. The work presented here provides a significant contribution to the field by successfully bridging the gap between discrete experimental measurements and continuous numerical simulations through a 240-node pixelized data analysis. This study has shown that while the numerical model maintains a robust MAE of 0.89°C relative to internal mesh samples, localized variances in boundary regions, specifically in the upper tray levels highlight the ongoing complexity of resolving turbulent transport phenomena in dense arrays. It is important to emphasize that these findings provide a validated benchmark for the eco-design and virtual testing of commercial ovens, significantly reducing the industry's reliance on costly physical prototypes. However, the findings of this study suggest that further research is required to fully elucidate the transient effects of the initial thermal boundary layer development near the burner assembly. Future investigations should aim to incorporate the dynamic responses of moving grids and varying product moisture contents to achieve even higher levels of spatial uniformity.

In summary, this research provides a validated methodology that enhances the understanding of heat distribution mechanisms, ultimately allowing manufacturers to minimize energy consumption while maximizing the sensory attributes and shelf-life of baked products.

5. ACKNOWLEDGMENTS

The authors would like to express their sincere gratitude to Inoksan for their invaluable support throughout this research. Special thanks are extended for providing the industrial oven equipment and technical documentation necessary for the experimental phase of this study. Their expertise in thermal engineering and industrial kitchen solutions was instrumental in the successful completion of the heat distribution analysis.

STATEMENTS AND DECLARATİONS

FUNDING

The authors declare that no funds, grants, or other financial support were received during the preparation of this manuscript.

COMPETING INTERESTS

The authors have no relevant financial or non-financial interests to disclose. While the study was supported by Inoksan (Bursa, Turkey) through the provision of technical support, equipment and facilities, the company had no role in the design of the study; in the collection, analyses, or interpretation of data; in the writing of the manuscript; or in the decision to publish the results.

REFERENCES

(1) Boulet, M., Marcos, B., Dostie, M., & Moresoli, C. (2010). CFD modeling of heat transfer and flow field in a bakery pilot oven. *Journal of Food Engineering*, *97*(3), 393–402. https://doi.org/10.1016/j.jfoodeng.2009.10.034

(2) Burhan, M., & Özalp, A. (2025). Analysis of temperature distribution in convection ovens using radial and tangential fans with different heat sources and air curtain designs. *Journal of the Faculty of Engineering and Architecture of Gazi University*, *40*(4), 2409–2424. https://doi.org/10.17341/gazimmfd.1669044

(3) Chhanwal, N., Anishaparvin, A., Indrani, D., Raghavarao, K. S. M. S., & Anandharamakrishnan, C. (2010). Computational fluid dynamics (CFD) modeling of an electrical heating oven for bread-baking process. *Journal of Food Engineering*, *100*(3), 452–460. https://doi.org/10.1016/j.jfoodeng.2010.04.030

(4) Fahey, M., Wakes, S., & Shaw, C. (2008). Use of computational fluid dynamics in domestic oven design. *The International Journal of Multiphysics*, *2*(1), 37–58. https://doi.org/10.1260/175095408784300216

(5) Ismail, O. S., Awonusi, A. A., & Akinoso, R. (2021). Isothermal air flow investigation in industrial baking oven of different impeller locations using Computational Fluid Dynamics (CFD) approach. *Journal of Engineering Science*, *17*(2), 73–91. https://doi.org/10.21315/jes2021.17.2.5

(6) Mittal, M., & Kumar, A. (2024). Numerical study of airflow and heat transfer in an industrial forced convection oven. International Journal of Thermal Sciences.

(7) Moukalled, F., Mangani, L., & Darwish, M. (2016). Implementation of boundary conditions in the finite-volume pressure-based method—Part I: Segregated solvers. Numerical Heat Transfer, Part B: Fundamentals, 69(6), 534–562. https://doi.org/10.1080/10407790.2016.1138748

(8) Purlis, E., & Salvadori, V. O. (2009). Modelling the browning of bread during baking. *Food Research International*, *42*(7), 865–870. https://doi.org/10.1016/j.foodres.2009.03.007

(9) Rek, Z., Rudolf, M., & Zun, I. (2012). Application of CFD simulation in the development of a new generation heating oven. Strojniški vestnik – Journal of Mechanical Engineering, 58(2), 134–144. https://doi.org/10.5545/sv-jme.2011.163

(10) Szpicer, A., Bińkowska, W., Stelmasiak, A., Zalewska, M., Wojtasik-Kalinowska, I., Piwowarski, K., Piepiórka-Stepuk, J., & Półtorak, A. (2025). Computational fluid dynamics simulation of thermal processes in food technology and their applications in the food industry. Applied Sciences, 15(1), 424. https://doi.org/10.3390/app15010424

(11) Therdthai, N., Zhou, W., & Adamczak, T. (2004). Three-dimensional CFD modelling and simulation of the temperature profiles and airflow patterns during a continuous industrial baking process. Journal of Food Engineering, 65(2), 211–217. DOI: 10.1016/j.jfoodeng.2004.02.026

(12) Turnow, J. (2018, February 22). *Heat transfer in OpenFOAM* [Training handout]. silentdynamics GmbH.

(13) Verboven, P., Scheerlinck, N., De Baerdemaeker, J., & Nicolaï, B. M. (2000a). Computational fluid dynamics modelling and validation of the isothermal airflow in a forced convection oven. Journal of Food Engineering, 43(1), 41–53.

(14) Verboven, P., Scheerlinck, N., De Baerdemaeker, J., & Nicolaï, B. M. (2000b). Computational fluid dynamics modelling and validation of the temperature distribution in a forced convection oven. Journal of Food Engineering, 43(1), 61–73.

(15) Versteeg, H. K., & Malalasekera, W. (1995). A review of the finite volume method for the numerical solution of the Navier-Stokes equations. *Journal of Computational Physics*, *112*(1), 1-23. https://doi.org/10.1006/jcph.1995.1001

(16) Williamson, G. G., & Wilson, D. I. (2007). Optimization of a gas-fired radiant burner for industrial tunnel ovens. Journal of Food Engineering, 82(2), 134–142. DOI: 10.1016/j.jfoodeng.2008.08.004

(17) Yan, Z., Chen, M., Chen, H., & Zhang, Y. (2024). Optimization of the temperature field inside a forced convection oven. AHFE International, DOI: 10.54941/ahfe1004503

(18) Zhou, W., & Therdthai, N. (2018). Three-Dimensional CFD Modeling of Continuous Industrial Baking Process. Computational Fluid Dynamics in Food Processing, CRC Press, 193–224. DOI: 10.1201/9781351263481-9